Accepted Manuscript

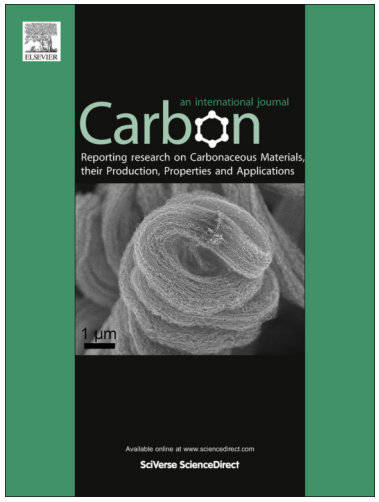

Dispersible Percolating Carbon Nano-electrodes for Improvement of Polysulfide Utilization in Li-S Batteries

Qingcong (Ray) Zeng, Feng Li, Ian R. Gentle, Hui-Ming Cheng, Da-Wei Wang

PII: S0008-6223(15)00441-8
DOI: http://dx.doi.org/10.1016/j.carbon.2015.05.044
Reference: CARBON 9938

To appear in: *Carbon*

Received Date: 13 March 2015
Accepted Date: 14 May 2015

Please cite this article as: Zeng, Q., Li, F., Gentle, I.R., Cheng, H-M., Wang, D-W., Dispersible Percolating Carbon Nano-electrodes for Improvement of Polysulfide Utilization in Li-S Batteries, *Carbon* (2015), doi: http://dx.doi.org/10.1016/j.carbon.2015.05.044

Dispersible Percolating Carbon Nano-electrodes for Improvement of Polysulfide Utilization in Li-S Batteries

Qingcong (Ray) Zeng [a], *Feng Li* [b], *Ian R. Gentle* [a], *Hui-Ming Cheng* [b], *Da-Wei Wang* [c,*]

[a] *School of Chemistry and Molecular Biosciences, University of Queensland, St Lucia Brisbane, QLD 4072, Australia*

[b] *Shenyang National Laboratory for Materials Science, Institute of Metal Research, Chinese Academy of Sciences, Shenyang, 110016, China*

[c] *School of Chemical Engineering, The University of New South Wales, UNSW Sydney, NSW 2052, Australia*

Email address: da-wei.wang@unsw.edu.au

Abstract

Percolating carbon nanoparticles were added into electrolyte to improve the performance of Li-S batteries. These percolating carbon nanoparticles acted as dispersible nanosized electrodes, allowed the direct electrochemical utilization of dissolved polysulfides in electrolyte, and mitigated the polysulfide shuttle. As a result, the polysulfide utilization was improved with the virtual sulfur capacity increasing from 538 mA h g^{-1} to 1270 mA h g^{-1}. The increment in high plateau-sloping capacity is 43 % while a much more significant 158 % increment is observed in low plateau region. The percolating carbon nanoparticles also improved the battery stability.

1. Introduction

High-density energy storage technologies are critical for future grids with renewable, yet intermittent, solar or wind plants. Among several types of new generation post-lithium-ion batteries, Li-S batteries are envisaged as promising high-energy batteries. Sulfur is a low-cost, non-toxic and abundant petroleum by-product. Sulfur cathode has a high theoretical capacity (1675 mA h g^{-1}) that is an order of magnitude higher than that of intercalation cathodes. The extraordinary capacity of sulfur compensates for the relatively small working voltage (~2 V) of Li-S batteries allowing a theoretical specific energy around 2600 Wh kg^{-1}, which is very competitive compared to conventional Li-ion batteries. However, the Li-S technology needs improvement in regards of cycle life, stability and utilization efficiency of active materials. The common performance-limiting factors include (i) high resistivity of sulfur and Li_2S_2/Li_2S that reduces voltage efficiency of cathodes, (ii) high solubility and shuttle effect of polysulfides that reduce material utilization efficiency, (iii) anode corrosion due to sulfide deposits.

Among these obstacles, the major issue is the polysulfide dissolution, which leads to the low utilization of active sulfur. To tackle with this problem, many strategies have been employed to constrain dissolved polysulfides. Carbon materials with various nanostructures, morphologies, porous textures, and surface functionalities have been widely investigated.[1-17] The synergy between physical and chemical interactions helps to confine sulfur.[8] Many polymers (conducting polymers or insulating binders) can be used to retain polysulfides.[11, 12] Apart from the synthesis of new materials, a different strategy is to constrain the recharge capacity or voltage of cathode.[13] Designing new Li-S battery structure is also popular. For example, carbon or hybrid interlayer, carbon-

coated separator or cation exchange membranes are developed to hinder polysulfide diffusion.[14-21] All in all, the mostly studied is highly porous or functionalized materials that could physically adsorb or chemically attract polysulfides. But the loss of polysulfides cannot be fully prevented due to their high solubility; and the scenario is even worse when sulfur percentage in cathode is high.

Alternatively, modifying the properties of electrolyte provides promising approaches to regulate polysulfide shuttle. For example, solvent-in-salt electrolyte and solid polymer electrolytes have been developed.[22, 23] Later, to avoid the issues like low lithium ion conductivity and high viscosity of polymer electrolytes, polysulfide salts were used as an electrolyte additive to buffer for polysulfide shuttle and compensate for the loss of sulfur in cathode.[24-26] Unlike chemically modifying the electrolytes, a new concept is using percolating electrolyte for Li/Polysulfide flow batteries.[27] This method allows the direct electrochemical utilization of dissolved polysulfides in electrolyte. Nevertheless whether or not the percolating electrolyte can be applied in normal Li-S batteries is unknown.

We prepared herein a percolating electrolyte with highly concentrated carbon nanoparticles for Li-S batteries. The concentrated carbon nanoparticles increased the electrolyte viscosity. The viscous electrolyte will hardly penetrate through the double-layer separator (Figs. 1A and 1B). Hence, the percolating electrolyte can be safely used in a Li-S cell. Our results showed the greatly enhanced performance of Li-S cells with this percolating electrolyte.

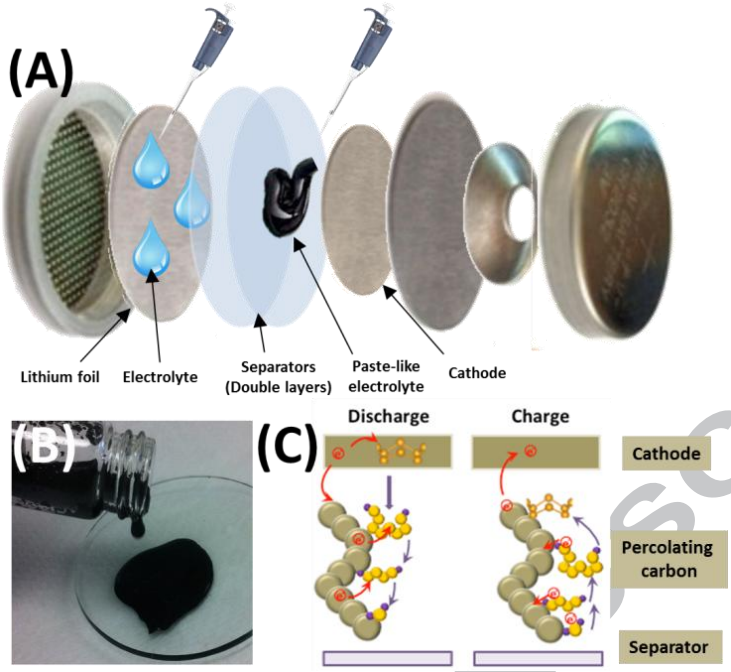

Figure 1. (A) Scheme showing the assembly of coin cell with paste-like electrolyte in cathode side. (B) Image of paste-like percolating electrolyte. (C) Schematic of Li-S batteries with a paste-like electrolyte containing percolating carbon nanoparticles.

2. Experimental Section

2.1 Materials

Carbon nanoparticles (CNPs) and polyvinylidene fluoride (PVDF) were used as provided. The electrolyte, 1 M bis(trifluoromethane) sulfonimide lithium (LiTFSI) salt in 1,3-dioxolane (DOL) and 1,2-dimethoxyethane (DME) (1:1 vol), was provided by GuoTaiHuaRong Co. Ltd. Elemental sulfur, N-methyl pyrrolidinone (NMP) , lithium sulfide (Li_2S), lithium nitrate ($LiNO_3$) were used as purchased from Sigma-Aldrich.

2.2 Preparation of cathode

Elemental sulfur and CNPs were firstly mixed together by grinding with a 7:3 weight ratio. Then the mixture was sealed into a glass vessel and heated in nitrogen-filled tube furnace at 155 °C for 12 h. Cathodes were prepared by a slurry coating method. The slurry was composed with 80 wt% of sulfur-carbon composite, 10 wt% conducting agent, 10 wt% PVDF as a binder and NMP as a solvent. The slurry was coated onto aluminium foil and was dried in a vacuum oven at 60 °C for 12 h. The thickness of the coating layer was 11 μm and the areal density was 1 mg/cm^2. The diameter of electrode was 9.5 mm and the weight of composite was around 0.7 mg.

2.3 Fabrication of electrolyte with percolating carbon nanoparticles

CNPs were dried in a vacuum oven at 120 °C overnight before transferring into glove box. The percolating electrolytes with two concentrations (4 mg mL^{-1} and 8 mg mL^{-1}) were prepared by dispersing CNPs in the commercial electrolyte under the assistance of ultrasonication (Hielscher ultrasonic probe) in the glove box.

2.4 Cell assembly and electrochemical measurement

The 2032 coin cells were assembled in an argon-filled glove box (MBraun UniLab) with a lithium anode and a polypropylene separator (Fig. 1A). The purchased electrolyte was 1 M bis(trifluoromethane) sulfonimide lithium (LiTFSI) salt in 1,3-dioxolane (DOL) and 1,2-dimethoxyethane (DME) (1:1 vol) with 0.1 M $LiNO_3$ as additive. The purchased electrolyte was used as an anolyte and the percolating electrolyte was used on cathode side. The volumes of electrolyte on anode side and cathode side were 10 μL and 30 μL, respectively. The mass of CNPs was 0.12 mg (4 mg mL^{-1}) or 0.24 mg (8 mg mL^{-1}), and the corresponding areal amount loading of CNPs based on cathode is 0.17 mg cm^{-2} and

0.34 mg cm^{-2}, respectively. For comparison, two blank cells were assembled. In both blank cells (BC-1/2), the percolating electrolyte on the cathode side was replaced with the same amount of pure electrolyte. In particular, an extra amount of 0.24 mg CNPs, equivalent to the amount of CNPs in 30 μL 8 mg mL^{-1} percolating electrolyte, was added into the cathode of BC-2, which resulted in a sulfur/carbon ratio of 49:51. The galvanostatic charge–discharge tests were conducted on LAND battery testing units. The current density and specific capacity were calculated based on the mass of sulfur in the cathode. The voltage window was 1.7-2.8 V vs. Li^+/Li^0. The current densities varied from 0.15 to 3 A g^{-1}. The cyclic voltammetry (CV) was measured between 1.7 to 2.8 V on Biologic VMP-3 electrochemical workstation at a scan rate of 0.1 mV s^{-1}. EIS measurements were conducted at the frequency range from 100 kHz to 10 mHz. A 500 μA current was applied to the H-cell.

2.5 Characterization

Transmission electron microscopy (TEM) images were taken on Philips Tecnai F20. X-ray photoelectron spectroscopy (XPS) was measured on a Kratos Axis Ultra spectrometer using Al Kα radiation (15 kV, 150 W). The survey spectra were recorded from 0 to 1000 eV at an energy interval of 1 eV/step. Porosity measurements were conducted on a Micromeritics Tristar II at 77 K after degassing overnight at 200 °C. X-ray diffraction (XRD) was collected on a Bruker D8 Advance X-Ray Diffractometer with a LynxEye detector and a Cu tube (40 kV, 40 mA). The CNPs/lithium polysulfide composites were sealed in an air-sensitive sample holder for XRD measurement. UV-Vis spectra were collected by Cary 60 UV-Vis spectrometer (Agilent Technologies) from 800 nm to 200

nm. Kinematic viscosity and dynamic viscosity of the percolating electrolyte were measured by using Cannon-Fenske-Routine viscometer (k=0.001832 $mm^2 s^{-2}$) at 25 °C.

3. Results and Discussions

Fig. 1C describes the interaction of polysulfides with CNPs in the percolating electrolyte. Since pure electrolyte is merely ionic conducting, the heterogeneous electron transfer to the polysulfides dissolved in electrolyte is via the diffusion of polysulfides towards the cathode and hence is rather slow. This slow kinetics results in the low utilization of sulfur. The percolating carbon nanoparticles in the electrolyte transport electrons throughout the cathode chamber to reduce the dissolved polysulfides (discharge) or to oxidize the sulfides (charge). Therefore the usable polysulfide percentage becomes higher, and the cathode capacity increases. Nanoporous carbon materials with high surface area are able to adsorb a large amount of polysulfides. We deliberately used carbon nanoparticles with small surface area (69 m^2/g, Fig. 2A) to minimize the interference from physical adsorption. The particle size of chosen CNPs is around 50-100 nm and they interconnect with each other forming a percolating network (Fig. 2B). Note that the oxygen content of these CNPs is extremely low (undetectable by XPS, Fig. 2C) ruling out the strong chemical interaction of sulfur and (poly)sulfides with oxygen functional groups. The kinematic viscosity and dynamic viscosity of 8 mg mL^{-1} paste-like electrolyte is 6.78 $mm^2 s^{-1}$ and 8.34 mPa s, eight times more viscous than water (Fig. 2D). It is assumed that, upon the discharge of sulfur, the low adsorption capacity of CNPs will not physically constrain a significant amount of polysulfides. Therefore the performance improvement can be ascribed to the polysulfides utilized by carbon nanoparticles.

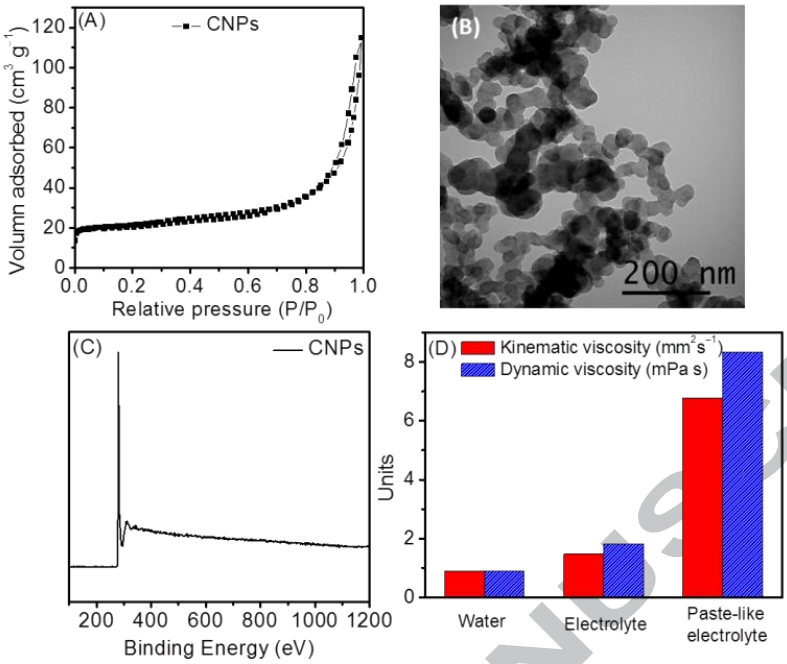

Figure 2. (A) Nitrogen adsorption–desorption isotherms of CNPs, (B) TEM image showing the size of CNPs and the formed percolating carbon network, (C) XPS spectrum of CNPs showing the oxygen-free feature and (D) Viscosity test results of 8 mg mL^{-1} percolating electrolyte with the comparison of pure electrolyte and water at 25 °C.

UV/Vis spectroscopy has been used to measure polysulfide solutions.[28-30] In this study, it was applied to characterize the sulfide species that were present in anolyte. Consequently the light absorption of the anolyte is an indicator that verifies whether the percolating carbon nanoparticles can reduce the polysulfide shuttle across the separator. Fig. 3 compares the light transmittance of anolytes from two different H-cells. One of the H-cells used pure electrolyte on the cathode side; the other one used percolating electrolyte in cathode chamber. The photographs of the anolyte sides of the H-cells that are fully discharged to 1.7 V are shown in the inset of Fig. 3. The anolyte from the H-cell with percolating electrolyte appeared greenish (Anolyte I, in red square) while the

anolyte from the H-cell with pure electrolyte was dark red (Anolyte II, in blue square). The colourful species dissolved in the anolyte indicated the existence of polysulfides in electrolyte even at the end of discharge. A similar result was observed by Li et al.[30] This result explained why the utilization of sulfur in Li-S batteries is often low.

Patel's results demonstrated the dependence of light absorption on the chain length and concentration of polysulfides.[29] Qualitatively the short-chain polysulfides (Li_2S_x, $x<4$) tend to absorb light at lower wavelength compared to the long-chain polysulfides; and the weaker absorption was observed at lower concentration. The Anolyte I completely absorbed the light at wavelength under 450 nm; and the characteristic absorption peak was around 540 nm (red curve in Fig. 2). The Anolyte II absorbed light at wavelength under 490 nm; and the characteristic absorption peak was around 550 nm (blue curve in Fig. 2). For comparison, the pure electrolyte absorbed lights at wavelength under 300 nm (black curve in Fig. 2). The higher absorption wavelength of Anolyte II suggested the longer chain of polysulfides (likely Li_2S_8 as the major constituent) and the lower transmittance, i.e. higher absorbance, reflected the larger concentration of polysulfides in Anolyte II. On the other side, the higher transmittance of Anolyte I suggested the lower concentration of short-chain polysulfides (possibly Li_2S_{2-4}). Sulfur reduction occurs along a cascade of polysulfides with gradually shortened chain length; and a portion of the dissolved polysulfides transfers across the separator to the anolyte side. The enrichment of short-chain polysulfides in Anolyte I signified the higher percentage of reduced long-chain polysulfides by the percolating CNPs in the electrolyte. In fact, the percolating electrolyte changed to brownish after re-charge, which is a clear sign that the sulfur

species were recovered. This result indicated the increased utilization of total sulfur via the electrochemical capture of dissolved polysulfides.

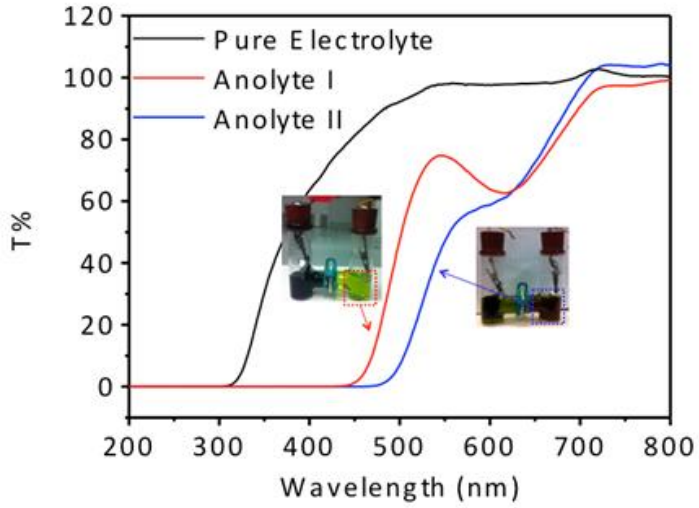

Figure 3. UV/Vis spectra of the pure electrolyte (black), Anolyte I from an electrolytic cell with percolating electrolyte (red), and Anolyte II from an electrolytic cell with pure electrolyte (blue). The pure electrolyte is 1 M LiTFSI in DOL/DME (1:1 vol) with 0.1 M $LiNO_3$. Inset shows the photographs of the two H-cells, where the anolyte chambers are highlighted in squares.

The initial cyclic voltammetry (CV) curves of the cells using the percolating electrolyte are shown in Fig. 4A, compared with a control cell using the pure electrolyte (BC-1). As seen in Fig. 4, the currents of the cells increased with the increase of CNPs concentration from 0 to 8 mg mL^{-1}. The CV profiles of the cells with percolating electrolytes showed characteristic cathodic peaks. The cathodic peak I centred at 2.3 V corresponded to the sulfur reduction to long-chain polysulfides and the cathodic peak II centred at 2.0 V corresponded to the conversion of long-chain soluble molecules to the insoluble Li_2S_2 or Li_2S. The larger cathodic peak area suggested the higher utilization of dissolved

polysulfides in percolating electrolyte. Note that the anodic peak area also increased compared to the control cell. The charge transfer resistance was reduced by a factor of 4~6 for the cells with percolating electrolytes according to the electrochemical impedance in Fig. S1.

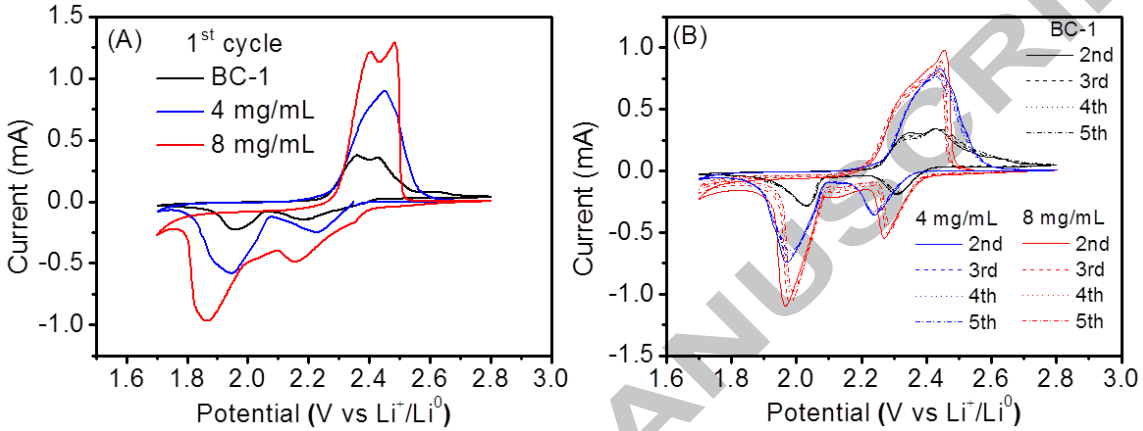

Figure 4. (A) The initial cyclic voltammetry curves of the cells and (B) 2nd-5th cycles CV plots with the comparison with the first blank cell (BC-1).

Rate performance was evaluated from 0.15 to 3 A g^{-1} as shown in Fig. 5A-D. The discharge/charge potential difference (ΔE) at different current densities was plotted in Fig. 5E. For BC-1, the ΔE at 0.15 A g^{-1} current density was already as high as 237.7 mV and increased to 472.8 mV with the current density increasing to 1.5 A g^{-1}. Such a high potential difference suggested a large cell resistance and sluggish electrochemical kinetics. The percolating carbon nanoparticles can efficiently reduce the potential difference. The ΔE at 0.15 A g^{-1} was reduced to 204.5 mV in the 4 mg mL^{-1} cell and to 181 mV in the 8 mg mL^{-1} cell. Even when the current density was increased to 3 A g^{-1}, the ΔE was 376.4 mV in the 4 mg mL^{-1} and 322.1 mV in the 8 mg mL^{-1} cell, even lower than that of the BC-1 at 1.5 A g^{-1}. BC-2 showed slightly better kinetics than BC-1, but

was still worse than the cells with percolating electrolytes. The results indicated the better reaction kinetics enabled by the percolating carbon nanoparticles.

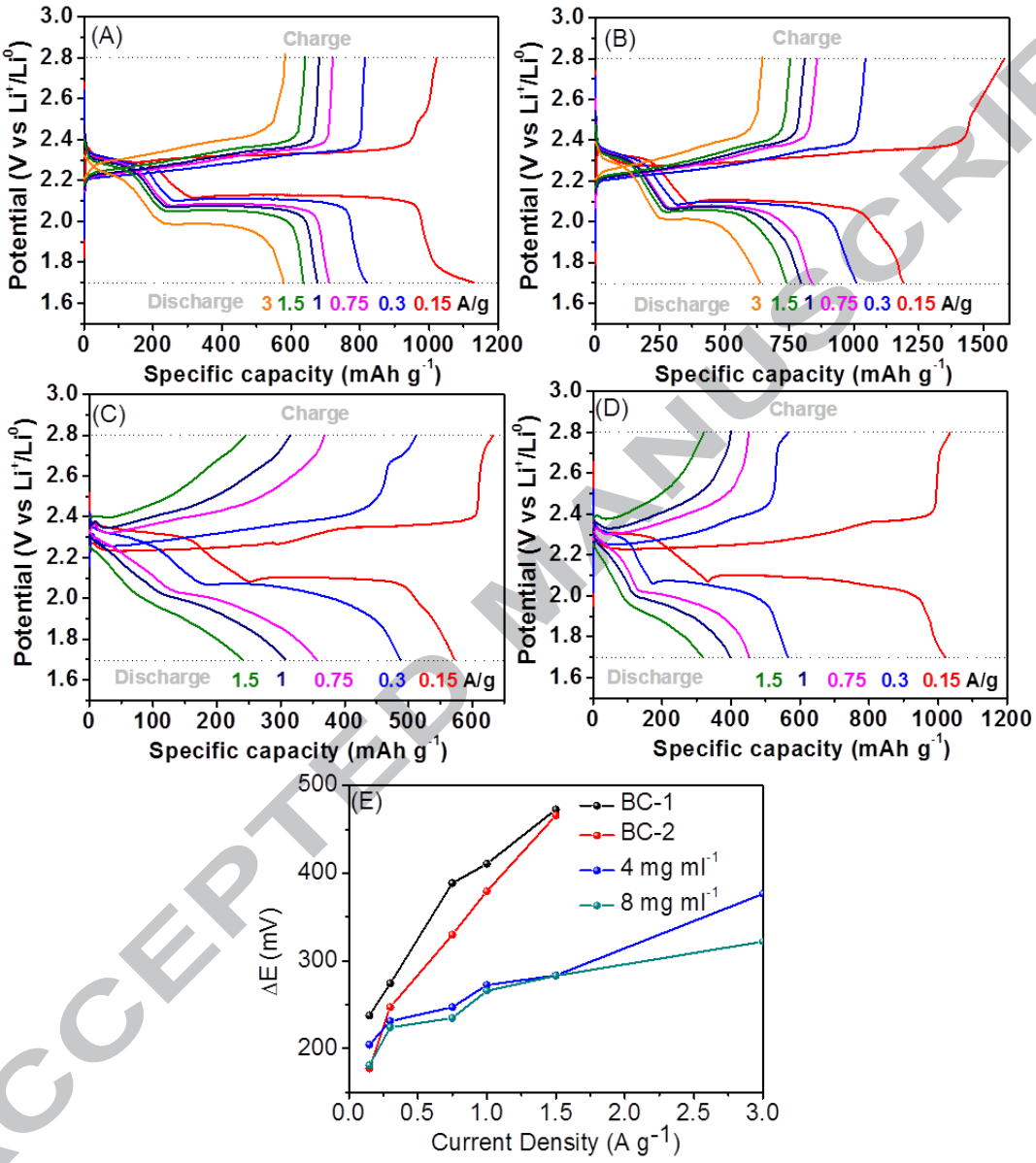

Figure 5. Discharge-charge profiles of (A) 4 mg mL^{-1} cell (B) 8 mg mL^{-1} cell (C) BC-1 (D) BC-2. (E) Discharge-charge potential difference (ΔE) at various current densities.

The discharge capacity of sulfur can be divided to two parts: the high plateau-sloping region capacity (Q_H) attributable to the formation of long-chain polysulfides (S_x^{2-} with $x \geq 4$) and the low plateau capacity (Q_L) assigned to the reduction of long-chain polysulfides. The theoretical capacities of Q_H and Q_L are 419 mA h g^{-1} and 1256 mA h g^{-1}, respectively.[24] Note that a virtual total capacity of about 1256 mA h g^{-1} for sulfur was suggested, which was mainly ascribed to the incomplete reduction of S_4^{2-} to S^{2-}.[31] This assumption is reasonable accounting for the coloured anolytes as shown in Fig. 3. Therefore, a value of 837 mA h g^{-1} is recommended for the virtual Q_L.[31] The Q_H and Q_L values are compared in Fig. 6A and B. At 0.15 A g^{-1}, the Q_H value increased from 252 mA h g^{-1} (BC-1) to 362 mA h g^{-1} (8 mg mL^{-1} cell), with the sulfur utilization ratio (against 419 mA h g^{-1}) increasing from 60.1% to 86.4%. The high plateau-sloping region reactions include the initial transformation of solid sulfur to the liquid S_8^{2-} anions (209.5 mA h g^{-1}) and the subsequent reduction of S_8^{2-} anions to S_4^{2-} anions (209.5 mA h g^{-1}). In the first plateau, solid-solid interaction between carbon and sulfur is crucial while the second plateau is more sensitive to polysulfide shuttle due to the high solubility and shuttle of S_8^{2-} anions. The strong shuttle effect and the lack of percolating nanoparticles reduced the accessible Q_H in the BC-1 but the higher carbon content in BC-2 helped with polysulfide utilization giving rise to higher Q_H. The percolating CNPs were able to reduce polysulfides in electrolyte, and hence, resulted in larger Q_H. More significant increment was observed in Q_L during which process the shuttling is predominant. At 0.15 A g^{-1}, the Q_L value increased from 320 mA h g^{-1} (BC-1) to 825 mA h g^{-1} (8 mg mL^{-1} cell), with the sulfur utilization ratio (against 837 mA h g^{-1}) increasing from 38.2% to 98.6% by more than two folds. The same trend was noticeable for the 4 mg mL^{-1} cell and

for a wide range of current densities. However the increment of Q_H and Q_L capacities in BC-2 cell at current densities above 0.15 A g^{-1} were very limited. This result indicated that percolating carbon nanoparticles can utilize dissolved polysulfide much more efficiently compared with those embedded in cathode. The total capacity of sulfur in the cells with percolating electrolytes approached to 600 mA h g^{-1} at 3 A g^{-1} (Fig. 6C). Appreciable stability was noticed in the cells with percolating electrolytes at 0.75 A g^{-1} (Fig. 6D). The ~99% coulombic efficiency suggested the reversible polysulfide reduction/oxidation on the dispersible CNPs in percolating electrolyte (Fig. S2).

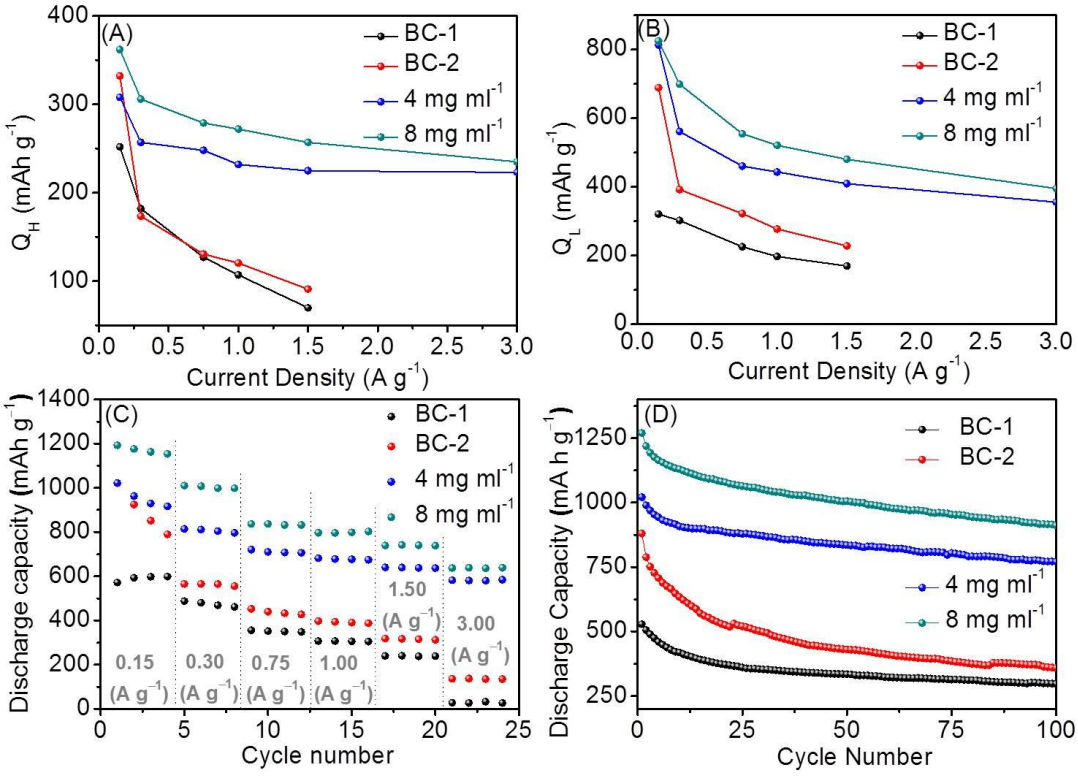

Figure 6. Comparison of (A) high plateau discharge capacities (Q_H) and (B) low plateau discharge capacities (Q_L) at different current densities. (C) Discharge capacity at different current densities and (D) Cycle stability measured at 0.75 A g^{-1}.

Air-sensitive X-ray powder diffraction was carried out to determine the discharge and recharge products in the percolating electrolytes (Fig. 7). The customized sample holder is shown in Fig. S3. The prominent broad peaks in both discharged and recharged electrolytes originated from CNPs and sample holder. The strongest diffraction peak for Li_2S was identified in the discharged percolating electrolyte; and the peak for S was detected in the recharged percolating electrolyte. On account of the weak XRD signals, it is postulated that the Li_2S or S was likely amorphous or nanocrystalline. On the other side, the polysulfide intermediates may exist in percolating electrolytes because of incomplete reaction, although no corresponding signals were resolved from XRD due to their amorphous nature (Fig. S4).[31, 33] This result is consistent with previous studies that distinct XRD peaks for sulfur species were only observed in solid carbon/sulfur cathodes, rather than in polysulfide electrolytes.[34] TEM characterization of the recovered CNPs from percolating electrolyte did not reveal any visible crystals or particles that might be attributable to either Li_2S or S (Fig. S5).

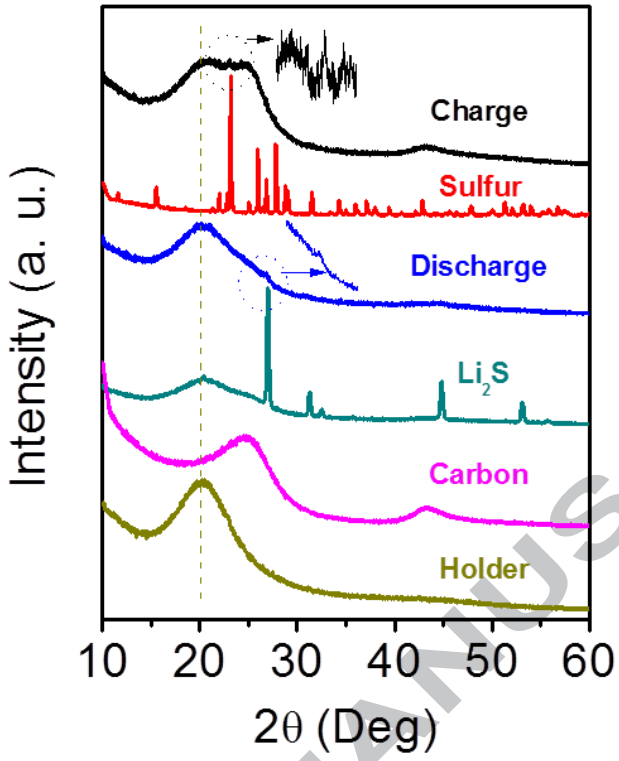

Figure 7. X-ray diffraction of carbon nanoparticles recovered from the discharged and recharged percolating electrolyte.

A possible mechanism is proposed to understand the working function of percolating carbon nanoparticles (Fig. 8). The reduction of sulfur on the cathode will first produce S_8^{2-}, while other soluble anions (S_6^{2-} and S_4^{2-}) are formed at higher depth of discharge. In our proof of concept attempt, nonporous carbon nanoparticles were used as conducting additive on the cathode. The very low surface area and porosity can only accommodate limited amount of soluble sulfur species. As a consequence, a majority of the as-produced soluble polysulfide anions will immediately escape into the electrolyte and diffuse towards the anode side. This process could be out of control if no barrier to polysulfide shuttling is in place and would lead to a quick performance fading. From the UV-vis observation of the glass H-cell filled with a percolating electrolyte (Fig. 3), we know that

only short chain polysulfides were able to migrate through the separator and into the anode chamber. On the contrary, a large portion of long chain polysulfides appeared in the anode chamber without percolating electrolyte. This indicates that the ongoing reduction of long chain polysulfides (like S_8^{2-}) by percolating carbon nanoparticles. Because the polysulfide anions diffuse while being reduced, this 'dynamic' reduction of 'moving objects' will form a gradient distribution of long polysulfides (higher solubility) close to the cathode surface and short polysulfides (low solubility) or sulfides (insoluble) close to the separator, as illustrated in Fig. 8. The sulfur migration across the separator is thus alleviated because a majority of the highly soluble polysulfides has been reduced before reaching the separator. As a result, the percolating electrolyte could hinder the polysulfide shuttling and increase the virtual sulfur capacity.

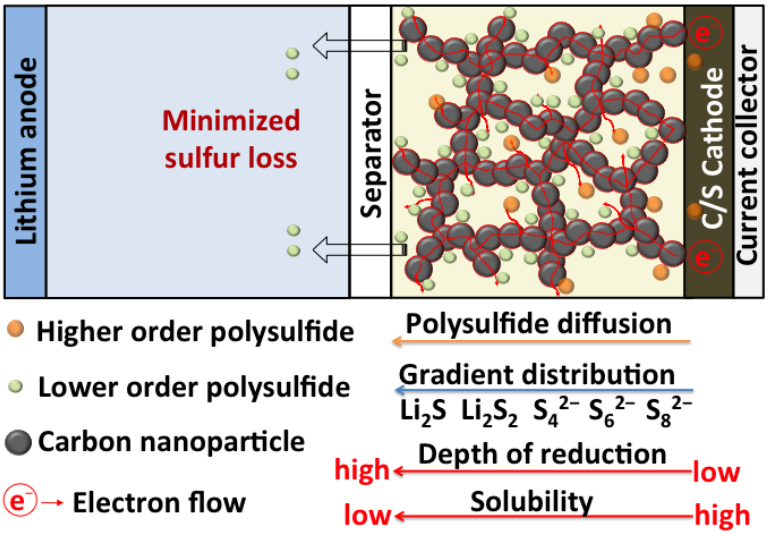

Figure 8. Schematic illustration of the gradient distribution of sulfur species in percolating electrolyte.

4. Conclusion

We demonstrated the improved Li-S battery performance by replacing a normal electrolyte with a percolating electrolyte that contains concentrated dispersible carbon nanoparticles. The percolating carbon nanoparticles act like dispersible nanosized electrodes and hence can reduce dissolved polysulfides during discharge and oxidize sulfide precipitates during recharge. The reversible utilization of escaped sulfur species in electrolyte helps to increase the overall cathode capacity by a factor of two. This approach also alleviates polysulfide shuttling because a majority of highly soluble polysulfides are converted to less soluble species before they can penetrate through the separator. This strategy is simple yet effective and opens a new avenue to fabricate high-performance Li-S batteries.

Acknowledgement

We acknowledge the financial support from UNSW Australia and The University of Queensland. D.W.W. acknowledges the support from UNSW FRG/ECR scheme. The authors acknowledge the facilities, and the scientific and technical assistance of from Australian Microscopy & Microanalysis Research Facility at the Centre for Microscopy and Microanalysis, The University of Queensland.

References

[1] Ji XL, Lee KT, Nazar LF. A highly ordered nanostructured carbon-sulphur cathode for lithium-sulphur batteries. Nat Mater 2009;8(6):500-6.

[2] Wang HL, Yang Y, Liang YY, Robinson JT, Li YG, Jackson A, et al. Graphene-Wrapped Sulfur Particles as a Rechargeable Lithium-Sulfur Battery Cathode Material with High Capacity and Cycling Stability. Nano Lett 2011;11(7):2644-7.

[3] Sun XG, Wang XQ, Mayes RT, Dai S. Lithium-Sulfur Batteries Based on Nitrogen-Doped Carbon and an Ionic-Liquid Electrolyte. Chemsuschem 2012;5(10):2079-85.

[4] Zhang CF, Wu HB, Yuan CZ, Guo ZP, Lou XW. Confining Sulfur in Double-Shelled Hollow Carbon Spheres for Lithium-Sulfur Batteries. Angew Chem Int Edit 2012;51(38):9592-5.
[5] Zhao MQ, Liu XF, Zhang Q, Tian GL, Huang JQ, Zhu WC, et al. Graphene/Single-Walled Carbon Nanotube Hybrids: One-Step Catalytic Growth and Applications for High-Rate Li-S Batteries. ACS Nano 2012;6(12):10759-69.
[6] Li Z, Huang Y, Yuan L, Hao Z, Huang Y. Status and prospects in sulfur–carbon composites as cathode materials for rechargeable lithium–sulfur batteries. Carbon 2015;92(0):41-63.
[7] Wang DW, Zeng QC, Zhou GM, Yin LC, Li F, Cheng HM, et al. Carbon-sulfur composites for Li-S batteries: status and prospects. J Mater Chem A 2013;1(33):9382-94.
[8] Zeng QC, Wang DW, Wu KH, Li Y, de Godoi FC, Gentle IR. Synergy of nanoconfinement and surface oxygen in recrystallization of sulfur melt in carbon nanocapsules and the related Li-S cathode properties. J Mater Chem A 2014;2(18):6439-47.
[9] Wu HB, Wei S, Zhang L, Xu R, Hng HH, Lou XW. Embedding Sulfur in MOF-Derived Microporous Carbon Polyhedrons for Lithium–Sulfur Batteries. Chem Euro J 2013;19(33):10804-8.
[10] Wang Z, Dong Y, Li H, Zhao Z, Bin Wu H, Hao C, et al. Enhancing lithium–sulphur battery performance by strongly binding the discharge products on amino-functionalized reduced graphene oxide. Nat Commun 2014;5.
[11] Xiao LF, Cao YL, Xiao J, Schwenzer B, Engelhard MH, Saraf LV, et al. A Soft Approach to Encapsulate Sulfur: Polyaniline Nanotubes for Lithium-Sulfur Batteries with Long Cycle Life. Adv Mater 2012;24(9):1176-81.
[12] Wang JL, Yao ZD, Monroe CW, Yang J, Nuli Y. Carbonyl-beta-Cyclodextrin as a Novel Binder for Sulfur Composite Cathodes in Rechargeable Lithium Batteries. Adv Funct Mater 2013;23(9):1194-201.
[13] Su YS, Fu YZ, Cochell T, Manthiram A. A strategic approach to recharging lithium-sulphur batteries for long cycle life. Nat Commun 2013;4.
[14] Su YS, Manthiram A. A new approach to improve cycle performance of rechargeable lithium-sulfur batteries by inserting a free-standing MWCNT interlayer. Chem Commun 2012;48(70):8817-9.
[15] Zhou GM, Pei SF, Li L, Wang DW, Wang SG, Huang K, et al. A Graphene-Pure-Sulfur Sandwich Structure for Ultrafast, Long-Life Lithium-Sulfur Batteries. Adv Mater 2014;26(4):625-31.
[16] Chung SH, Manthiram A. High-Performance Li-S Batteries with an Ultra-lightweight MWCNT-Coated Separator. J Phys Chem Lett 2014;5(11):1978-83.
[17] Chung SH, Manthiram A. A hierarchical carbonized paper with controllable thickness as a modulable interlayer system for high performance Li-S batteries. Chem Commun 2014;50(32):4184-7.
[18] Huang JQ, Zhang Q, Peng HJ, Liu XY, Qian WZ, Wei F. Ionic shield for polysulfides towards highly-stable lithium-sulfur batteries. Energy Environ Sci 2014;7(1):347-53.
[19] Zhou G, Zhao Y, Zu C, Manthiram A. Free-standing TiO2 nanowire-embedded graphene hybrid membrane for advanced Li/dissolved polysulfide batteries. Nano Energy 2015;12(0):240-9.
[20] Yao H, Yan K, Li W, Zheng G, Kong D, Seh ZW, et al. Improved lithium-sulfur batteries with a conductive coating on the separator to prevent the accumulation of inactive S-related species at the cathode-separator interface. Energy Environ Sci 2014;7(10):3381-90.
[21] Huang J-Q, Zhuang T-Z, Zhang Q, Peng H-J, Chen C-M, Wei F. Permselective Graphene Oxide Membrane for Highly Stable and Anti-Self-Discharge Lithium–Sulfur Batteries. ACS Nano 2015;9(3):3002-11.

[22] Suo LM, Hu YS, Li H, Armand M, Chen LQ. A new class of Solvent-in-Salt electrolyte for high-energy rechargeable metallic lithium batteries. Nat Commun 2013;4.
[23] Hayashi A, Ohtomo T, Mizuno F, Tadanaga K, Tatsumisago M. All-solid-state Li/S batteries with highly conductive glass-ceramic electrolytes. Electrochem Commun 2003;5(8):701-5.
[24] Yang Y, Zheng GY, Cui Y. A membrane-free lithium/polysulfide semi-liquid battery for large-scale energy storage. Energy Environ Sci 2013;6(5):1552-8.
[25] Chen SR, Dai F, Gordin ML, Wang DH. Exceptional electrochemical performance of rechargeable Li-S batteries with a polysulfide-containing electrolyte. RSC Adv 2013;3(11):3540-3.
[26] Zhang SS, Read JA. A new direction for the performance improvement of rechargeable lithium/sulfur batteries. J Power Sources 2012;200:77-82.
[27] Fan FY, Woodford WH, Li Z, Baram N, Smith KC, Helal A, et al. Polysulfide Flow Batteries Enabled by Percolating Nanoscale Conductor Networks. Nano Lett 2014;14(4):2210-8.
[28] Barchasz C, Molton F, Duboc C, Lepretre JC, Patoux S, Alloin F. Lithium/Sulfur Cell Discharge Mechanism: An Original Approach for Intermediate Species Identification. Anal Chem 2012;84(9):3973-80.
[29] Patel MUM, Demir-Cakan R, Morcrette M, Tarascon JM, Gaberscek M, Dominko R. Li-S Battery Analyzed by UV/Vis in Operando Mode. Chemsuschem 2013;6(7):1177-81.
[30] Li YJ, Zhan H, Liu SQ, Huang KL, Zhou YH. Electrochemical properties of the soluble reduction products in rechargeable Li/S battery. J Power Sources 2010;195(9):2945-9.
[31] Mikhaylik YV, Akridge JR. Polysulfide shuttle study in the Li/S battery system. J Electrochem Soc 2004;151(11):A1969-A76.
[32] Su YS, Manthiram A. Lithium-sulphur batteries with a microporous carbon paper as a bifunctional interlayer. Nat Commun 2012;3.
[33] Fu YZ, Su YS, Manthiram A. Li2S-Carbon Sandwiched Electrodes with Superior Performance for Lithium-Sulfur Batteries. Adv Energy Mater 2014;4(1).
[34] Canas NA, Wolf S, Wagner N, Friedrich KA. In-situ X-ray diffraction studies of lithium-sulfur batteries. J Power Sources 2013;226:313-9.